A study of the structural phase transitions in AlF_3: X-ray powder diffraction, differential scanning calorimetry (DSC) and Raman scattering investigations of the lattice dynamics and phonon spectrum

1990 J. Phys.: Condens. Matter 2 5663

(http://iopscience.iop.org/0953-8984/2/26/003)

J. Phys.: Condens. Matter 2 (1990) 5663–5677. Printed in the UK

A study of the structural phase transitions in AlF_3: x-ray powder diffraction, DSC and Raman scattering investigations of the lattice dynamics and phonon spectrum

Ph Daniel†, A Bulou†, M Rousseau†, J Nouet†, J L Fourquet‡, M Leblanc‡ and R Burriel§

† Laboratoire de Physique de l'Etat Condensé, CNRS URA 807, Université du Maine, Faculté des Sciences, 72017 Le Mans Cédex, France

‡ Laboratoire des Fluorures et Oxyfluorures Ioniques, CNRS URA 449, Université du Maine, Faculté des Sciences, 72017 Le Mans Cédex, France

§ Facultad de Ciencia, ICMA, Universidad de Zaragoza–CSIC, 50009 Zaragoza, Spain

Received 18 July 1989, in final form 7 December 1989

Abstract. The cubic–rhombohedral phase transition at 450 °C of AlF_3 is studied by DSC, x-ray powder diffraction and Raman scattering. It is demonstrated that the transition is of first order with a hysteresis of about 6 degrees. It is established by x-ray powder diffraction patterns that the room temperature space group is $R\bar{3}c$. A temperature study of the Raman scattering spectra (that confirms the above conclusion) evidences the presence of two soft modes. It is shown from group theory that the transition can be imputed to the condensation of the R_5 mode of the cubic Brillouin zone and the attribution of the Raman lines is deduced on the basis of the compatibility diagram between the cubic and rhombohedral symmetries. The frequencies of the Raman lines are used to adjust the parameters of a rigid ion model and to calculate the phonon spectrum in the cubic phase. The calculated phonon density of states appears to be strongly dependent on the soft phonon frequency.

1. Introduction

In recent years, structures built using MF_6 octahedra have been the object of a great number of investigations in the framework of phase transitions and lattice dynamics. They mainly concern systems with octahedra linked together either three dimensionally like in fluoroperovskites $A'M''F_3$ (Shapiro *et al* 1972, Rousseau *et al* 1977) or two dimensionally in the $A'M'''F_4$ compounds (Bulou and Nouet 1982, 1987). MF_6 octahedra can be considered as rigid entities and the structural phase transitions can be imputed either to MF_6 octahedra tilts or to MF_6 octahedra sheets gliding (Launay *et al* 1985, Bulou *et al* 1989a). However, in spite of the number of studies, several problems such as the central peak in the neutron scattering spectra are still unsolved.

AlF_3 is also made of MF_6 octahedra three-dimensionally linked together and undergoes a structural phase transition: in the high-temperature phase AlF_3 is cubic, isomorphous to ReO_3, but becomes rhombohedral at room temperature due to octahedra

0953-8984/90/265663 + 15 $03.50

rotating around their three-fold axis. This system is a 'pure octahedra system' and so its behaviour could provide information about the origin and the mechanism of the phase transitions in fluoroperovskites and fluoroaluminates. The importance of this system also comes from the fact that many other MF_3 compounds exhibit the same kind of transition.

Moreover the calculation of the lattice dynamics in aluminium fluoride requires only a small number of parameters therefore the force constants and the whole phonon spectrum can be predicted by Raman scattering data alone. This is of great interest for the study of the phase transition since single crystals are difficult to grow thus precluding inelastic neutron scattering studies. Moreover AlF_3 is one of the simplest systems which can be prepared in the amorphous state. In this framework the knowledge of the vibrational spectrum of crystallised AlF_3 and of the interionic forces constants are very useful.

In this paper the room temperature structure of AlF_3 is reinvestigated by x-ray powder diffraction and the lattice dynamics properties are studied by Raman scattering. A rigid ion model is proposed to describe the phonon spectrum in the cubic phase and the parameters of the model are deduced from Raman scattering data.

2. X-ray powder diffraction and DSC investigations

2.1. X-ray powder diffraction investigation

The crystal structure of aluminium fluoride has been the object of conflicting studies: many authors (Staritzky and Asprey 1957, Hanic and Stempelova 1962, Hoppe and Kissel 1984, Ravez and Mogus-Milankovic 1984) have established that AlF_3 is rhombohedral at room temperature but the space group has never been determined unambiguously.

Knowledge of crystal symmetry is essential for a vibrational study so we have reinvestigated the structure of aluminium fluoride in the room temperature phase by x-ray powder diffraction.

The sample was prepared from Al_2O_3 and NH_4HF_2 in excess giving $(NH_4)_3AlF_6$. Then AlF_3 is obtained by thermal decomposition of $(NH_4)_3AlF_6$ at 700 °C during 20 hours under argon atmosphere. X-ray diffraction patterns of AlF_3 were collected on a D501 Siemens diffractometer with the use of copper radiation. The angular range was $2\theta = 10°–130°$ with steps of 0.04°. Refinements were performed with a Rietveld program modified by A Lebail (Gibaud *et al* 1986, Lartigue *et al* 1987).

Like other trifluorides (Jack and Gutmann 1951, Hepworth *et al* 1957) the extinctions are consistent with the space group $R\bar{3}c$; the other space groups, R32 and $R\bar{3}$, previously proposed by Staritzky and Asprey, and Hoppe and Kissel respectively, cannot be accepted since reflections *hhl* with $l = 2n + 1$ that characterise the space groups $R\bar{3}$ or R32 are never observed. Note that the existence of such lines was not mentioned by either authors. It can be concluded that aluminium fluoride exhibits a rhombohedral symmetry with space group $R\bar{3}c$. This space group of the room temperature phase is a subgroup of the $Pm\bar{3}m$ space group of the high-temperature phase, and the rhombohedral phase originates from the cubic phase mainly by rotation of octahedra around their three-fold axis.

Table 1 summarises the lattice and structural parameters. Each aluminium atom occupies the centre of a slightly distorted octahedron formed by six fluorine atoms with

Table 1. Lattice and structural parameters of AlF_3 at 300 K determined by x-ray powder profile refinement (with copper radiation). The R factors (reliability factors) are classically defined by $R_i = 100\Sigma|I_{obs} - SI_{calc}|/\Sigma|I_{obs}|$ with I_{obs} and I_{calc} the integrated intensities of reflections and S the scale factor. Profile intensity: $R_P = 100\Sigma|Y_{obs} - SY_{calc}|/\Sigma|Y_{obs}|$. Weighted profile: $R_w = 100\sqrt{\Sigma(W(Y_{obs} - SY_{calc}))^2/\Sigma(WY_{obs})^2}$. The vibrational coefficients relate to the expression: $T = \exp[-(B_{11}h^2 + B_{22}k^2 + B_{33}i^2 + 2B_{12}hk + 2B_{13}hl + 2B_{23}kl)]$. Standard deviations are given in parentheses.

	R (%)			Hexagonal cell ($Z = 6$)		Rhombohedral cell ($Z = 2$)	
T (K)	R_i	R_p	R_w	a (Å)	c (Å)	a_R (Å)	α_R (deg)
300	2.56	9.79	11.62	4.9305(6)	12.4462(7)	5.0314(2)	58.6772(2)

		x	y	z	B_{11}	B_{22}	B_{33}	B_{12}	B_{13}	B_{23}
Al	6b	0	0	0	0.0117(1)	$B_{22} = B_{11}$	0.0010(1)	0.0059(3)	0	0
F	18e	0.4275(2)	0	0.25	0.0150(1)	0.019(1)	0.0017(1)	0.0098(6)	0	0

Al–F = 1.797(3) Å which is consistent with the sum of ionic radii (1.82 Å). The F–F distance is 2.542 Å. The F–Al–F angle is 90.02(6)° and Al–F–Al = 157.07(7)°. So we deduce that the angle of rotation, ω, of octahedra around the three-fold axis is ω = 13.99(1)°, which is large compared to usual octahedral tilt angles in perovskites or fluoroaluminates. However this is one of the smallest tilt angles encountered in the MF_3 family (Ravez and Mogus-Milankovic 1985).

2.2. DSC investigations

The existence of a phase transition has been checked by differential scanning calorimetry. Experiments have been performed using a Perkin–Elmer DSC 4 and for data

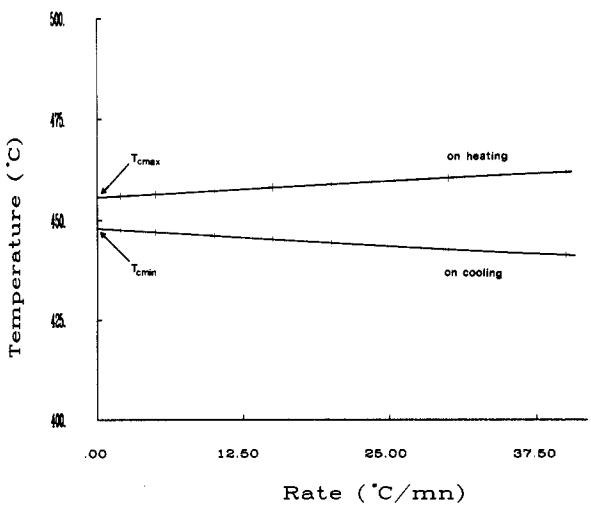

Figure 1. T_{peak} as a function of the rate R on cooling and heating in the DSC analysis. $T_{c_{max}}$ = 456 °C, $T_{c_{min}}$ = 448 °C.

treatment with a Perkin–Elmer micro-computer. The sample used consists of aluminium fluoride powder recrystallised by heating AlF_3 in a sealed platinum crucible at 800 °C for 4 days. Measurements were carried out in closed aluminium cups over a temperature range from 430 to 480 °C with various rates of cooling and heating, R (2 °C min^{-1} to 40 °C min^{-1}) in order to determine exactly the transition temperature T_c. In fact the real temperature is given as a function of the observed temperature by a law of form

$$T_{real} = T_{obs} - CR + D$$

where C and D are constants dependent on the apparatus. The transition temperatures are deduced by extrapolation of the $T_{obs} = f(R)$ curves; $T_{c_{min}}$ on cooling and $T_{c_{max}}$ on heating (figure 1)

$$T_{c_{max}} = 456 \pm 0.5\,°C \qquad T_{c_{min}} = 448 \pm 0.5\,°C$$

In all the experiments a large endothermic peak has been observed with a large hysteresis (figure 2). This hysteresis establishes the real first-order character of the transition previously detected by other authors (Matthias 1950, Thakur *et al* 1952, Ravez and Mogus-Milankovic 1984). Note that such a hysteresis is not observed in perovskites or fluoroaluminates exhibiting the same kind of transition. The enthalpy of the transition is about 1.7(1) cal g^{-1}.

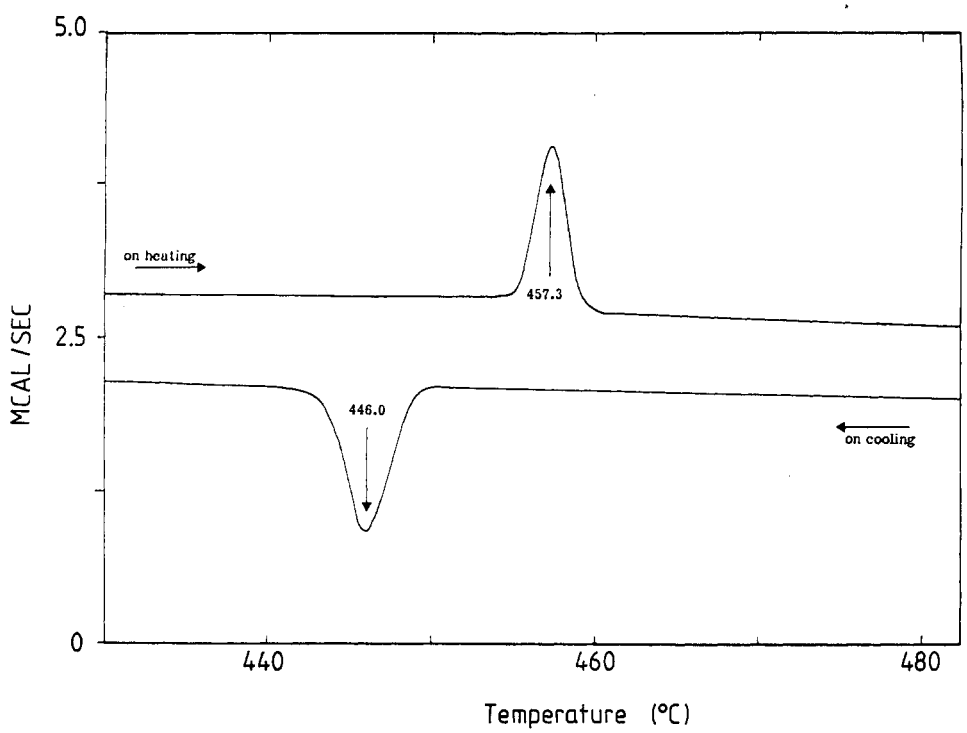

Figure 2. DSC diagram of AlF_3 at 10 °C min^{-1}.

3. The Raman scattering study

3.1. Experimental details

The Raman spectra were collected on a DILOR Z-24 single-channel triple monochromator coupled with a Coherent-Innova 90-3 argon ion laser. The 514.5 nm excitation line was chosen with an incident power not exceeding 1 W.

The samples consisted of single crystals grown either in the vapour phase (Ferey *et al* 1975) or by the flux technique (Wanklyn 1969). The size is more important in the second method—they are typically one mm^3. They have a cubic shape and in the experiments the laser beam always propagates along the tetragonal axis of the cubic phase. In any case, the crystal size is always small so the measurements have only been performed under microscope. The high-temperature experiments were realised with a heating stage Chaix-Meca between 20 °C and 550 °C.

3.2. Group theory analysis and experimental results

From group theory the optical normal modes of vibration at the centre of the Brillouin zone in the two phases can be classified as follows:

(i) in the cubic phase (high-temperature phase, $Pm\bar{3}m$ space group)

$$\Gamma_{opt} = \Gamma_9 + 2\Gamma_{10}$$

where Γ_9 and Γ_{10} are given in Kovalev (1965) notation. This notation will be used in this paper for all group theory considerations in the cubic phase. Γ_9 and Γ_{10} correspond respectively to F_{2u} and F_{1u} in the usual Mulliken notation;

(ii) in the rhombohedral phase (low-temperature phase, $R\bar{3}c$ space group)

$$\Gamma_{opt} = A_{1g} + 2A_{2g} + 3E_g + 2A_{1u} + 2A_{2u} + 4E_u.$$

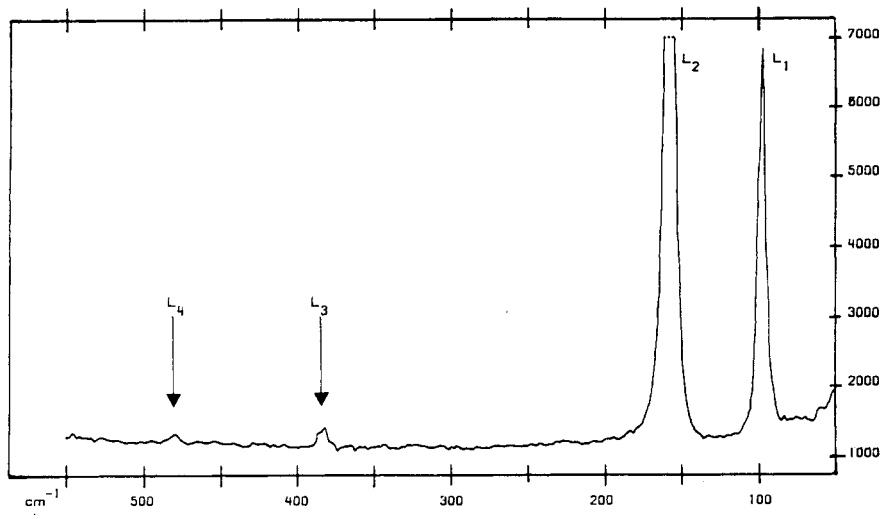

Figure 3. Room temperature Raman spectrum of AlF_3.

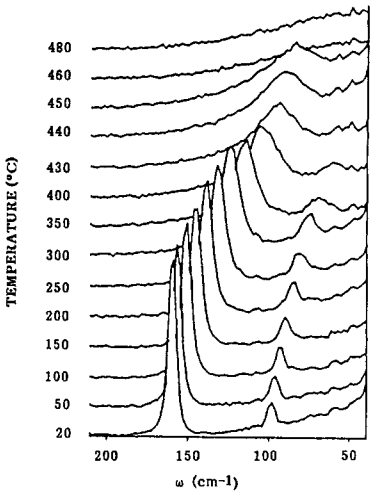

Figure 4. Temperature dependence of the Raman spectra of AlF_3.

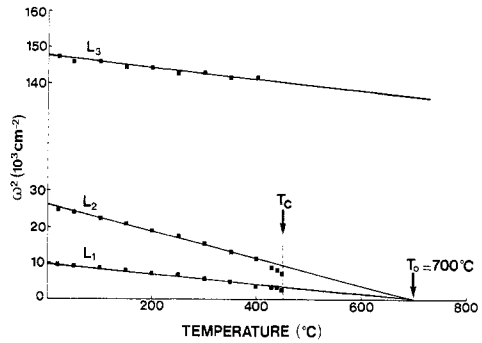

Figure 5. Square frequencies of L_1, L_2 and L_3 lines as a function of temperature.

No mode is Raman active in the cubic phase while in the rhombohedral phase the four A_{1g} and E_g symmetry modes are Raman active. In agreement with these predictions no Raman line is observed above T_c while the room temperature Raman spectrum exhibits four lines (figure 3) observed at 98, 158, 383 and 481 cm^{-1}. These results then are consistent with the $R\bar{3}c$ symmetry. Note that in the case of R32 or $R\bar{3}$ space groups, as previously proposed, a greater number of Raman lines would be expected.

When heating the samples the two lower frequency Raman lines decrease in frequency and in intensity (figure 4) while the third line undergoes only small changes and the last line is invariable. So the L_1 and L_2 lines could be assigned to soft modes of the structural phase transition; figure 5 shows that the temperature behaviour of their frequencies is fairly well described by a power law of Landau type:

$$\omega \approx (T_0 - T)^{1/2} \qquad (T_0 = 700\,°C)$$

Table 2. Compatibility diagrams of the symmetries between the rhombohedral Γ-point and the cubic Γ- and R-points.

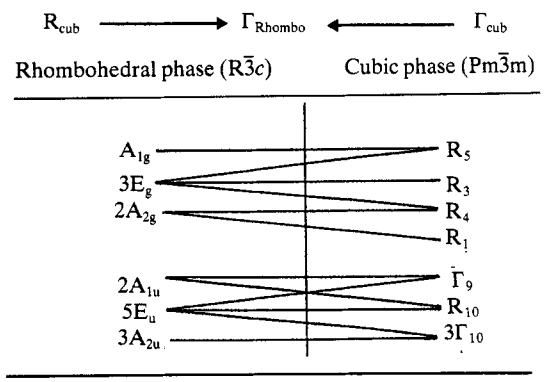

although T_0 is far above the transition temperature ($T_c \simeq 450$ °C). This result establishes that L_1 and L_2 really correspond to the soft modes of the transition. The frequency jump at T_c is consistent with the first-order character of the transition shown by DSC studies.

3.3. Attribution of the Raman lines

As shown in the preceding section, in the rhombohedral phase there are three E_g symmetry modes which cannot be distinguished from the group theory point of view. However, as often occurs, these modes may have different symmetry in the high-temperature phase. Most of them are only weakly affected by the transition (except the soft modes) and so any mode in the rhombohedral phase may be characterised by its corresponding symmetry in the cubic phase. The symmetry of the vibrational modes at the different points of the Brillouin zone of the cubic phase are given in the appendix together with the corresponding symmetry adapted eigenvectors as calculated from the projection operators. Moreover the superstructure lines which arise in the rhombohedral phase indicate that the phase transition can be imputed to the condensation of a zone boundary mode located at the $R(0.5, 0.5, 0.5)$ point of the cubic Brillouin zone and therefore the Γ modes of the rhombohedral phase arise from the Γ and R modes of the cubic one. The compatibility diagrams, as established from group–subgroup relations between $Pm\bar{3}m$ and $R\bar{3}c$ are presented in table 2. It is shown that the three E_g modes can be distinguished in the cubic phase. It appears that the transition can be imputed to the condensation of the R_5 mode (R_5 is given in Kovalev (1965) notation, it is indeed the so-called R_{25} mode which softens in perovskites) since only the soft mode gives rise to the A_{1g} symmetry mode in the low-temperature phase. The symmetry coordinates in the cubic phase at the R point of the Brillouin zone (see appendix) shows, as expected, that the R_5 mode corresponds to the octahedra rotation mode. Table 2 also shows that R_5 gives rise to two soft modes (A_{1g} and E_g symmetries) below the transition, in agreement with our experimental data. By comparison with the fluoroperovskites (Rousseau *et al* 1975), it can be predicted that the E_g mode corresponds to the lower frequency. The compatibility diagram also shows that the two other E_g symmetry modes in the rhombohedral room temperature phase come from the R_4 and R_3 modes of the cubic

Table 3. Attribution of the room temperature Raman lines of AlF_3. In parentheses are given the symmetry in the cubic phase according to Kovalev (1965) labelling.

	$E_g(R_5)$	$A_{1g}(R_5)$	$E_g(R_4)$	$E_g(R_3)$
ν (cm^{-1})	98	158	383	481

phase. From the symmetry coordinates (see appendix) it appears that the R_3 mode is a stretching mode and is therefore probably of a higher frequency than the R_4 distortion mode. This attribution is also deduced from the comparison to other MF_3 compounds (FeF_3, CrF_3 . . .) (Daniel *et al* 1990). The higher frequency mode is almost independent of the size of the octahedra while the other greatly decreases when the octahedra size increases. Obviously the distortions are easier when the fluorines are farther from one another, i.e. for large octahedra. Table 3 summarises the assignment proposed.

4. Calculation of the phonon spectrum in the cubic phase of aluminium fluoride

Knowledge of the phonon spectrum in the cubic phase of AlF_3 is needed so as to get information on the origin of the transitions. In the present case using a rigid ion model, the phonon spectrum depends on a small number of parameters which can be adjusted from Raman scattering data alone as measured in the rhombohedral phase since most of them are not strongly dependent on this structure. In the harmonic approximation the potential energy is defined by a sum of second-order terms. Moreover, neglecting the electronic polarisability, it is convenient to distinguish the long-range electrostatic forces from the short-range interaction between nearest-neighbour ions. The long-range part of the dynamical matrix is calculated with the help of a standard program and depends only on the atomic positions and on the effective ionic charges. Moreover the electrical neutrality $Z_{Al} + 3Z_F = 0$ has to be fulfilled.

The short-range dynamical matrix is determined for the case of axially symmetric forces. Thus it involves two parameters A_i, B_i, which correspond to the second derivative of the short-range potential function Φ_i, parallel and perpendicular to the line joining the interacting ions. These undimensionless coefficient are classically defined in the CGS system by

$$A_i = (2V/e^2)(\partial^2\Phi_i/\partial r_{i\parallel}^2) \qquad B_i = (2V/e^2)(\partial^2\Phi_i/\partial r_{i\perp}^2)$$

where e is the elementary charge ($e = 4.803 \times 10^{-10}$ CGS units). In the more appropriate MKS system, we use the following relation:

$$A_i = (8\pi\varepsilon_0 V/e^2)(\partial^2\Phi_i/\partial r_{i\parallel}^2) \qquad B_i = (8\pi\varepsilon_0 V/e^2)(\partial^2\Phi_i/\partial r_{i\perp}^2)$$

with $e = 1.602 \times 10^{-19}$ C.

In this system we define the A_i' and B_i' parameters, expressed in $N\,m^{-1}$, through the relation

$$A_i' = (e^2/8\pi\varepsilon_0 V)A_i = (\partial^2\Phi_i/\partial r_{i\parallel}^2) \qquad B_i' = (e^2/8\pi\varepsilon_0 V)B_i = (\partial^2\Phi_i/\partial r_{i\perp}^2).$$

In the present case there are two kinds of interactions and as found for alkali halides it will be assumed that $B_i = -A_i/10$ (Tosi 1964). Such an assumption has been used successfully to describe the fluorine–fluorine interaction for the calculation of the phonon spectrum of the fluoroperovskites (Rousseau *et al* 1977); a similar ratio has been found for the aluminium–fluorine interaction from the study of the phonon spectrum of $RbAlF_4$ (Bulou *et al* 1989b). So, in the case of cubic AlF_3 this model requires only three parameters: (i) the effective charge of the fluorine atoms (Z_F); (ii) the Al–F short-range interaction constant (A_1); and (iii) the F–F short-range interaction constant (A_2).

The two constants, A_1 and A_2, correspond to the so-called A_2, A_3 constants used in the description of the phonon spectrum of the perovskites. These three parameters can be deduced from the three Raman scattering frequencies (R_5, R_3, R_4). Since these modes appear only once in the decomposition in irreducible representations, their eigenvectors can be calculated from group theory (see appendix). The application of the dynamical matrix at the R-point to such eigenvectors then gives analytical expressions for the frequencies

$$\omega^2(R_3) = (e^2/VM_F)(A_1 + A_2 + 3B_2 + 6.773Z_F^2 + 34.270Z_{Al}Z_F) \tag{1}$$

$$\omega^2(R_4) = (e^2/VM_F)(B_1 + 2A_2 + 2B_2 + 22.693Z_F^2 - 10.852Z_{Al}Z_F) \tag{2}$$

$$\omega^2(R_5) = (e^2/VM_F)(B_1 + 4B_2 - 6.228Z_F^2 - 10.852Z_{Al}Z_F) \tag{3}$$

where V is the cubic cell volume, M_F the mass of a fluorine atom and e the elementary charge.

Therefore, assuming that the R_3 and R_4 frequencies are almost temperature independent and that the R_5 mode is of low frequency, it appears that Raman scattering data are sufficient to calculate the three parameters of the model and to predict the whole phonon spectrum. The parameters of the model are $A_1 = 92.41$, $B_1 = -0.924$, $A_2 = 7.90$, $B_2 = -0.790$, $Z_{Al} = 2.103$, and $Z_F = -0.701$ which corresponds to the following force constants: $A_1' = 236.25\ N\ m^{-1}$, $B_1' = -23.62\ N\ m^{-1}$, $A_2' = 20.20\ N\ m^{-1}$, and $B_2' = -2.02\ N\ m^{-1}$.

Of course since the number of data is the same as the number of adjusted parameters, the validity of the results cannot be checked. However, the force constants so deduced are in good agreement with the ones obtained from the studies of the tetrafluoroaluminate $RbAlF_4$ (Bulou *et al* 1989b). It can be noted also that the effective charges are very close to the ones obtained in this compound. If we suppose an opposite attribution for the E_g modes of the room temperature phase, coming from the R_3 and R_4 modes, the values of the force constants are not consistent with those obtained in fluoroperovskites and fluoroaluminates. Note that the analytical expressions of the soft mode R_5 depends only on the B_1 orthoradial constant of Al–F interaction. If we suppose that B_1 decreases (with parameters A_1, A_2, B_2, Z_F, Z_M fixed) we note a corresponding important variation of R_5 in the same sense. On the other hand, the R_4 mode only weakly decreases in frequency (figure 6). In the temperature study of the Raman spectra below the transition we

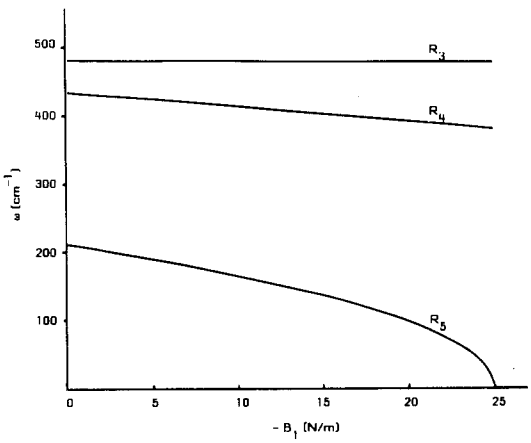

Figure 6. Variation of R-point mode frequencies as a function of the B_1 constant. Fixed parameters: $A_1 = 236.25\ N\ m^{-1}$; $A_2 = 20.20\ N\ m^{-1}$; $B_2 = -A_2/10$; $Z_F = -0.701$ ($Z_M = -2.103$).

observe that the $E_g(R_4)$ mode (at 383 cm^{-1} at room temperature) weakly decreases when heating the samples. This can be seen in figure 5 (L_3 line) where the square of the frequency (which is linear against the A_i, B_i parameters in the harmonic approximation) is plotted against temperature. This fact could be connected to the B_1 variation used to describe the R_5 softening, though such a frequency decrease occurs in any material at high temperature and in spite of the fact that the model results should be discussed only in the high temperature cubic phase. Nevertheless the decreasing of the B_1 constant is consistent with an increasing of the anharmonicity of the system.

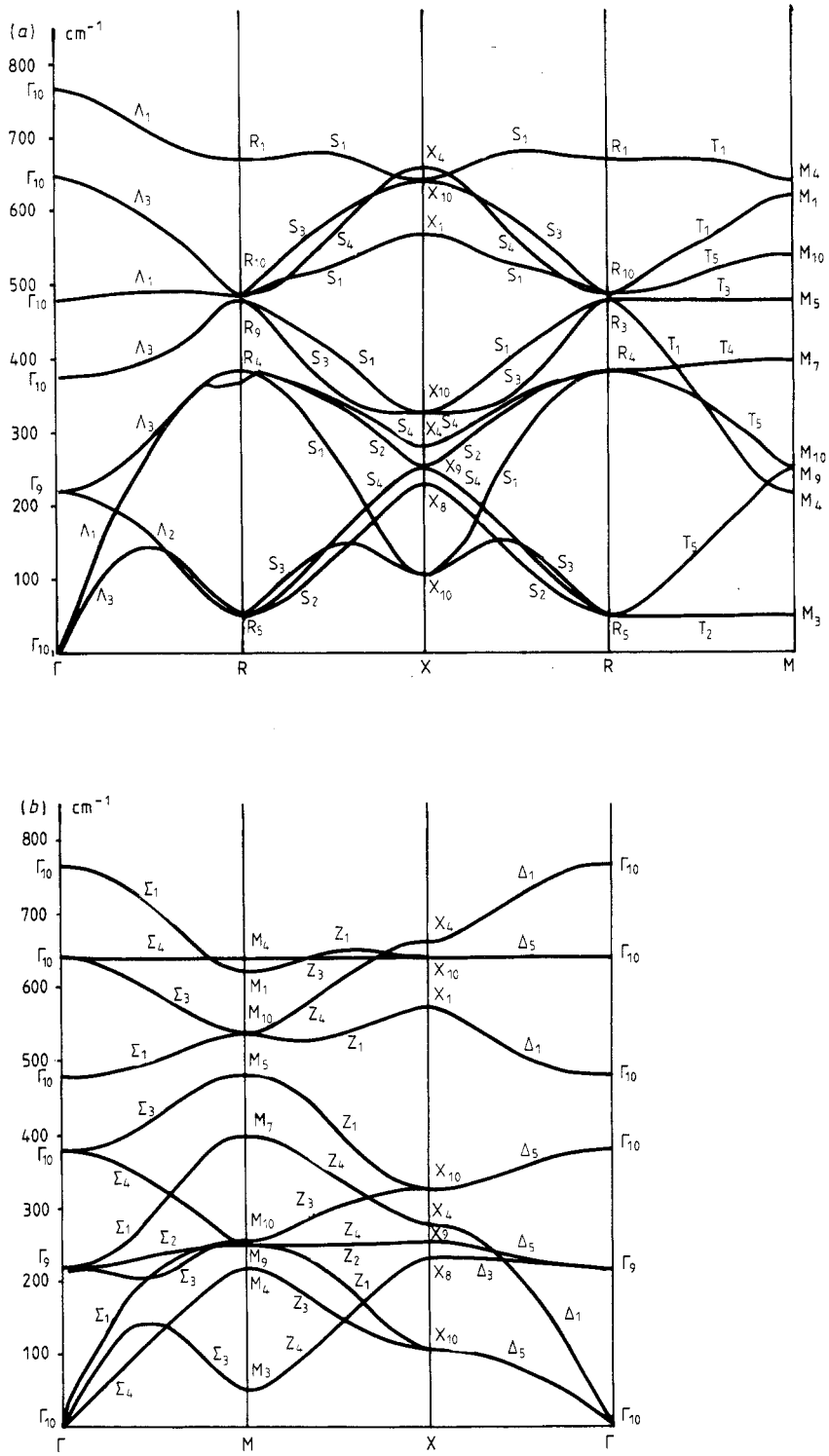

Figure 7. Calculated phonon spectrum: (*a*) Γ–R–X–R–M; and (*b*) Γ–M–X–Γ.

The calculated phonon spectrum is shown in figure 7. It appears that the phonon branch of T_2 symmetry (between R_5 and M_3), corresponding to octahedra rotations, is very flat, as occurs in perovskites (figure 7(*a*)). The analytical expression for the frequency of the M_3 mode is given by

$$\omega^2(M_3) = (e^2/VM_F)(B_1 + 4B_2 - 6.1505Z_F^2 - 10.852Z_{Al}Z_F). \tag{4}$$

From (3) and (4) we obtain

$$\omega^2(M_3) = \omega^2(R_5) + 0.0775(e^2/VM_F)Z_F^2. \tag{5}$$

From this last relation, we conclude that in a rigid ion model the frequency of the R-point mode is lower than the value at the M-point of the T_2 line. Then, in this case, the phonon spectrum could explain why the condensation occurs at the R-point rather than at the M-point. Moreover if we compare this relation with the one obtained in perovskites (Rousseau *et al* 1977) we observe that they are very similar, though slightly more important due to the fact that the octahedra are smaller and therefore the (very small) electric repulsion between fluorines is more efficient. However the difference remains negligible and the first-order character of the transition could be connected to the quasiflatness of the phonon branch as proposed for $RbAlF_4$ (Bulou *et al* 1989c).

Knowledge of the phonon spectrum makes it possible to predict some additional dynamical properties of AlF_3 such as the one-phonon density of state. It is calculated using a mesh of 10^6 $\boldsymbol{q}$ vectors in the 1/16th volume of the first Brillouin zone with a frequency interval of 1 cm^{-1}. The result is plotted in figure 8. We should note an abrupt change in the vicinity of 50 cm^{-1}, i.e. at the frequency of the R_5 mode. It has been checked that this singularity is exactly located at the value of the soft R_5 mode frequency.

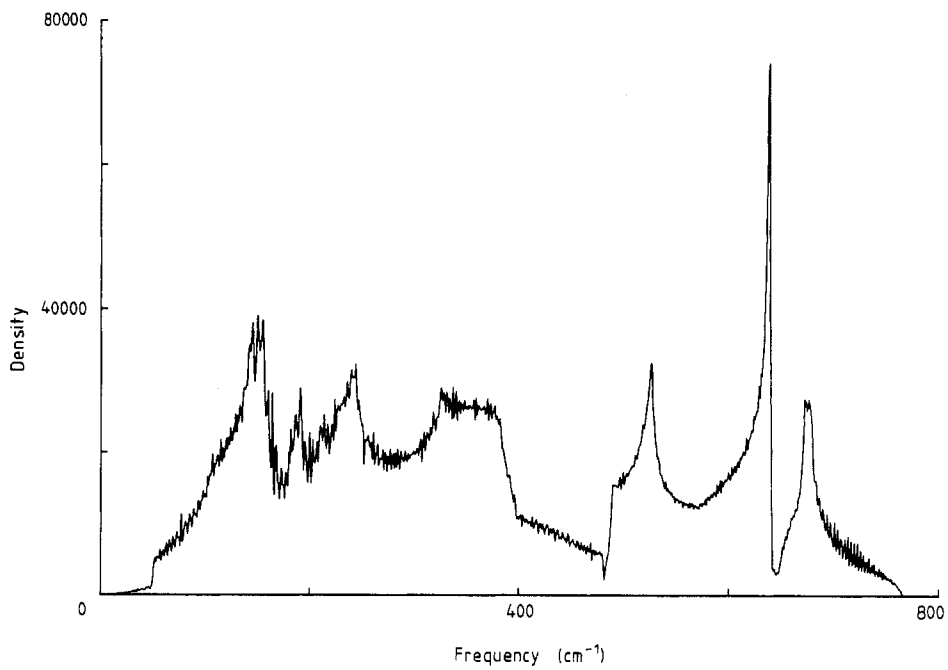

Figure 8. Calculated one-phonon density of state of AlF_3 in the cubic phase.

Thus in AlF_3 the soft mode plays a major role in the density of state. Moreover an intense peak is observed at 640 cm^{-1}; such fact can be attributed to the existence of a flat phonon branch along the line Γ_{10}–Σ_4–M_4–Z_3–X_{10}–Δ_5–Γ_{10} and indeed in the whole $\Gamma XM\Gamma$ plane. The normal coordinates of vibration of these modes are the same and are given by

$$\begin{array}{cccc} \text{Al} & F_1 & F_2 & F_3 \\ (0, 0, -0.55; & 0, 0, 0; & 0, 0, 0; & 0, 0, 0.83) \end{array}$$

It can be noted that Γ_{10}, which can be studied by infrared spectroscopy, belongs to this flat line.

5. Conclusions

To conclude, the first-order structural phase transition of AlF_3 at high temperature is confirmed and an important hysteresis is evidenced. The room temperature structure determined by x-ray powder diffraction has been shown to be $R\bar{3}c$ instead of R32 or $R\bar{3}$. The Raman scattering spectra in the low-temperature phase studied on single crystals under microscope are also consistent with $R\bar{3}c$ symmetry.

All the lines have been attributed on the basis of a group theory analysis in the cubic phase together with the establishment of compatibility diagrams between cubic and rhombohedral symmetries. This group theory analysis shows that the transition can be imputed to the condensation of the triply degenerate R_5 mode giving rise to two soft modes (A_{1g} and E_g symmetry) in the low-temperature phase. These two soft modes have been experimentally evidenced by a temperature study of the Raman scattering spectra. It can be noted that this 'perovskite-like structure' undergoes a real first-order transition with thermal hysteresis. The Raman scattering data have made possible the prediction of the whole phonon spectrum of AlF_3 in cubic symmetry with a rigid ion model involving three parameters. These parameters have been adjusted and they are in good agreement with the values determined from lattice dynamics studies of AMF_4 and AMF_3 compounds. It can be seen from the calculated phonon spectrum that the T_2 branch from R_5 to M_3 is quite flat as occurs in perovskite compounds. However the frequency of the R_5 mode is slightly lower than the M_3 mode strengthening the view that the transition is due to the condensation of the former mode. The density of state has also been calculated. It must be noted that in this compound the soft flat phonon branch from R_5 to M_3 causes an important discontinuity in the density of state; indeed the soft phonon frequency could be measured from the analysis of the density of state.

The method used in this work is a simple way to deduce the interionic force constants and predict the phonon spectrum of any MF_3 compound from Raman scattering data alone. This is useful in studies of the transitions of crystallised MF_3 and also in the analysis of the static and dynamic properties of amorphous MF_3. Such data are also essential to predict the phonon spectrum of layered AMF_4 compounds which undergo various kind of transitions.

Acknowledgments

The authors would like to thank G Niesseron for his contribution to sample preparation. A part of this work has been supported by a French–Spanish Integrated Action.

Appendix. Eigenvector symmetry in the cubic phase and compatibility diagrams

The symmetry of vibration modes in the cubic phase ($Pm\bar{3}m$–O_h^1) of aluminium fluoride is determined by the method proposed by Maradudin and Vosko (1968); it consists in

Table 4. Mode symmetries at high-symmetry points of the first cubic Brillouin zone (Kovalev (1965) labelling).

q symbol	q coordinates	$G(q)$	Irreducible representations (Kovalev labelling)
Γ	(0, 0, 0)	O_h	$\Gamma_9 + 3\Gamma_{10}$
R	(0,5, 0.5, 0.5)	O_h	$R_1 + R_3 + R_4 + R_5 + R_{10}$
M	(0.5, 0.5, 0)	D_{4h}	$M_1 + M_3 + 2M_4 + M_5 + M_7 + M_9 + 2M_{10}$
X	(0.5, 0, 0)	D_{4h}	$X_1 + 2X_4 + X_8 + X_9 + 3X_{10}$

the establishment of the $\mathbf{T}(q, S)$ matrix (matrix of the mechanical representation of the wave vector group associated to each S symmetry element of the group of the wave vector $G(q)$. They are reduced into irreducible representations $\tau(q)$ of $G(q)$ which are summarised in table 4 according to Kovalev (1965) labelling. The symbols used for lines

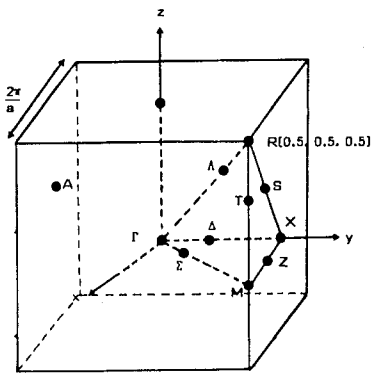

Figure 9. First cubic Brillouin zone. Lines and points of high symmetry.

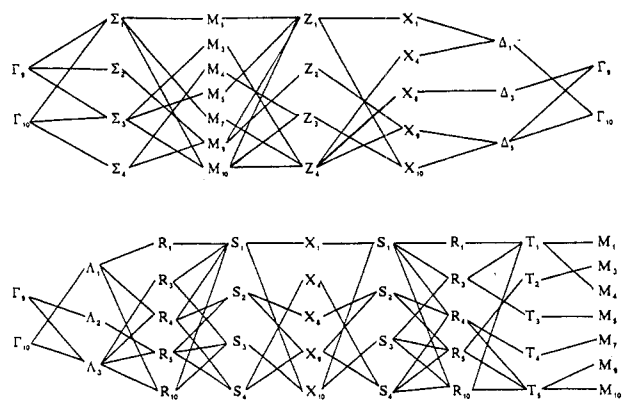

Figure 10. Compatibility diagrams.

Table 5. Symmetry coordinates at Γ, R, M and X points of the cubic Brillouin zone (Kovalev (1965) [1] and Koster (1957) [2] labelling).

	Al			F_1			F_2			F_3		
[1]/[2]	x	y	z	x	y	z	x	y	z	x	y	z
Γ_{25}/Γ_9					$1/\sqrt{2}$	$1/\sqrt{2}$	$1/\sqrt{2}$		$-1/\sqrt{2}$	$-1/\sqrt{2}$		
Γ_{15}/Γ_{10}	α	α	α	β	γ	γ	γ	β	γ	γ	γ	β
R_2'/R_1				$1/\sqrt{3}$				$1/\sqrt{3}$				$1/\sqrt{3}$
R_{12}'/R_3				$1/\sqrt{6}$ $1/\sqrt{2}$				$1/\sqrt{6}$ $-1/\sqrt{2}$				$-2/\sqrt{6}$
R_{15}/R_4				$1/\sqrt{2}$	$1/\sqrt{2}$		$1/\sqrt{2}$		$1/\sqrt{2}$	$1/\sqrt{2}$	$1/\sqrt{2}$	
R_{25}/R_5				$1/\sqrt{2}$	$1/\sqrt{2}$		$-1/\sqrt{2}$		$1/\sqrt{2}$	$-1/\sqrt{2}$	$-1/\sqrt{2}$	
R_{25}'/R_{10}	1	1	1									
X_2'/X_1												1
X_1/X_4			α			β			β			
X_3/X_8						$1/\sqrt{2}$			$-1/\sqrt{2}$			
X_5'/X_9				1		1						
X_5/X_{10}	α α	$-\alpha$ α		β β	γ γ		$-\gamma$ γ	$-\beta$ β				
M_4/M_1				$1/\sqrt{2}$				$1/\sqrt{2}$				
M_3/M_3					$1/\sqrt{2}$		$-1/\sqrt{2}$					
M_3'/M_4			α									β
M_4/M_5				$1/\sqrt{2}$				$-1/\sqrt{2}$				
M_1/M_7					$1/\sqrt{2}$		$1/\sqrt{2}$					
M_5/M_9						1			1			
M_5'/M_{10}	α α	$-\alpha$ α								β β	$-\beta$ β	

and points of high symmetry of the Brillouin zone are presented in figure 9. The symmetry adapted eigenvectors can be calculated by the projection operator method and they are given in table 5 for each high-symmetry point of the cubic Brillouin zone. Compatibility diagrams between high-symmetry lines and points in the Brillouin zone of the cubic phase are illustrated in figure 10.

References

Bulou A, Gibaud A, Debieche M, Nouet J, Hennion B and Petitgrand D 1989a *Phase Transitions* **14** 47
Bulou A and Nouet J 1982 *J. Phys. C: Solid State Phys.* **15** 183
—— 1987 *J. Phys. C: Solid State Phys.* **20** 2885
Bulou A, Rousseau M, Nouet J and Hennion B 1989b *J. Phys.: Condens. Matter* **1** 4553
Bulou A, Rousseau M and Nouet J 1989c *Ferroelectrics* at press
Daniel Ph, Bulou A, Leblanc M, Rousseau M and Nouet J 1990 *Phys. Rev.* B submitted for publication
Ferey G, Leblanc M, de Pape R, Passaret M and Bothorel-Razazi M P 1975 *J. Cryst. Growth* **29** 209
Gibaud A, Lebail A and Bulou A 1986 *J. Phys. C: Solid State Phys.* **19** 4623
Hanic F and Stempelova D 1962 *Acta Crystallogr. Acad. Sci. Hung.* **32** 309
Hepworth M A, Jack K H, Peacock R D and Westland G J 1957 *Acta Crystallogr.* **10** 63
Hoppe R and Kissel D 1984 *J. Fluorine Chem.* **24** 327
Jack K H and Gutmann V 1951 *Acta Crystallogr.* **4** 246
Koster G F 1957 *Solid State Physics* vol 5 (New York: Academic)
Kovalev O V 1965 *Irreducible Representations of the Space Groups* (New York: Gordon and Breach)
Lartigue C, Lebail A and Percheron A 1987 *J. Less-Common Met.* **129** 65
Launay J M, Bulou A, Hewat A W, Gibaud A, Nouet J and Laval J Y 1985 *J. Physique* **46** 173
Maradudin A A and Vosko S H 1968 *Rev. Mod. Phys.* **40** 1
Matthias B T 1950 *Helv. Phys. Acta* **23** 167
Ravez J and Mogus-Milankovic A 1985 *Japan J. Appl. Phys.* **24–2** 687
—— 1984 *Mater. Res. Bull.* **19** 1311
Rousseau M, Gesland J Y, Julliard J, Nouet J, Zarembowitch J and Zarembowitch A 1975 *Phys. Rev.* B **12** 1575
Rousseau M, Nouet J and Almairac R 1977 *J. Physique* **38** 107
Shapiro S M, Axe J D, Shirane G and Riste T 1972 *Phys. Rev.* B **6** 4332
Staritzky E and Asprey L B 1957 *Anal. Chem.* **29** 984
Thakur R L, Rock E J and Pepinsky R 1952 *Am. Mineral.* **37** 695
Tosi M P 1964 *Solid State Physics* vol 16 (New York: Academic)
Wanklyn B M 1969 *J. Cryst. Growth* **5** 279